Silicon (2018) 10:2577–2584
https://doi.org/10.1007/s12633-018-9793-4

ORIGINAL PAPER

Study of Undoped and Indium Doped ZnO Thin Films Deposited by Sol Gel Method

M. Medjaldi[1,3] · O. Touil[2] · B. Boudine[2] · M. Zaabat[3] · O. Halimi[2] · M. Sebais[2] · L. Ozyuzer[4]

Received: 23 February 2016 / Accepted: 28 February 2018 / Published online: 14 April 2018

Abstract
In this paper, we report the effects of Indium doping concentrations (from 0 to 10wt%) on the structural, morphological, and optical properties of deposited In doped ZnO (IZO) thin films prepared by the sol–gel method through the dip coating technique. X-ray diffraction (XRD) analysis indicates that all ZnO thin films have a polycrystalline nature with a hexagonal wurtzite phase with (002) as a preferential orientation. XRD results demonstrate that the particle size of ZnO decreased with the increase in Indium concentrations. Raman scattering spectra confirmed the wurtzite phase and the presence of intrinsic defects in our samples. Energy dispersive spectroscopy (EDS) and the X-ray photoelectron spectroscopy (XPS) measurements, confirmed the presence of zinc, oxygen and indium elements which is in agreement with XPS results. The photoluminescence (PL) spectra of the films exhibit defects-related visible emission peaks, with intensities differing owing to different concentrations of zinc vacancies. UV–Vis spectrometer measurements show that all the films are highly transparent in the visible wavelength region (≥70%) and presented two different absorption edges at about 3.21 eV and 3.7 eV, these may be correspond to the band gap of zinc oxide and indium oxide respectively.

Keywords IZO thin films · Raman · Phonon · Transmittance · Photoluminescence

1 Introduction

Transparent Conducting Oxides (TCOs) are extensively used in microelectronic devices, light emitting diodes, thin films, anti-reflection coatings for transparent electrodes in solar cells [1, 2], gas sensors in surface acoustic wave devices [3], varistors, spintronic devices, and lasers [4]. They perform in a very interesting way in optical, mechanical and electrical applications [5].

Among TCOs, ZnO has advantages of low cost and non-toxicity, so it has been acknowledged as a promising alternative to indium tin oxide and tin oxide [6]. ZnO easily crystallizes in the wurtzite structure with n-type electrical conductivity. It is a binary II-VI semiconductor compound, with a bulk direct band gap of 3.37eV at room temperature and a large exciton binding energy of 60meV. This could be increased to over 100meV in super lattices [7]. As a result of its high electrochemical stability and absence of toxicity, it is typically used in a variety of optical and electrical applications [8].

In spite of its excellent conductivity, as it contains high concentrations of native defects (oxygen vacancies or zinc interstitials), ZnO is not stable chemically and electrically at high temperature. However, its physical properties can be deeply modified and improved by n-type impurity doping, the doped ZnO thin films having low resistivity and suitable good optical gap energy at low temperature and being transparent in the visible region. ZnO nanostructures can doped with a variety of elements, like Al, Ga, Mg, Li, P, N, Ni, In, and Co [9–11]. IZO thin films have been selected as the object of this study because they exhibit high mobility, good optical transparency, and lower material cost.

Thin films can be developed by some physical methods, such as thermal evaporation [12], pulsed laser deposition (PLD) [13] and sputtering [14], or chemical techniques,

✉ M. Medjaldi
medjaldi.malika@gmail.com

1 Université Abbas Laghrour Khanchela, El Hamma, Khenchela, Algeria

2 Laboratoire de Cristallographie, Université frères Mentouri Constantine, Constantine, Algeria

3 Laboratoire des composants actifs et matériaux Université Larbi Ben M'hidi Oum El Bouaghi, El Bouaghi, Algeria

4 Izmir Institute of Technology, TR-35430 Izmir, Turkey

e.g. chemical vapor deposition (CVD) [15], spray pyrolysis [16] and sol–gel processes [17]. Among these, the sol–gel method has been chosen for of its simplicity, safety, and large area substrate coating. In this process, deposited films are transformed from amorphous to crystalline states by post annealing.

The crystallization behavior of ZnO thin films is affected by the ZnO solution concentration, the doping concentration, the type or the nature of the substrate, the conditions of the heat treatment, the film thickness, and the organic compounds [18]. The main objective of this study is to identify the best doping concentration which gives sol-gel deposited IZO thin films with the best semiconducting properties. For this reason, we have investigated the effects of a high Indium doped concentration (0.5, 5 and 10wt%) on the structural, morphological, and optical properties of IZO thin films prepared by the sol gel method and deposited by the dip coating technique on a glass subtract.

2 Experimental Procedure

2.1 Preparation of the solution

Before the deposition process, it is very important to have a transparent and stable sol. To prepare 0.17M of a undoped ZnO solution, 1.5g of zinc acetate dihydrate as a precursor was dissolved in 40ml of 2-methoxyethanol. When the solution turned milky, an equimolar amount of monoethanolamine (MEA) ($NH_2CH_2CH_2$-OH) was added as a stabilizer to obtain a clear and transparent solution after stirring at 60°C for 2h. The solution was aged for 24 hours. Indium chloride ($InCl_3$) was used as the Indium doping source. The mass doping rates were 0.5, 5 and 10wt%.

The undoped and doped films were deposited by the dip coating technique, at room temperature, in air, with a controlled withdrawal speed, on a cleaned glass substrate.

The samples were dried after each coating step in a furnace to evaporate and remove any organic residuals. The process of dip coating and drying was repeated 10 times in order to achieve the desired film thickness (Table 1). As a consequence, the resulting coatings are transparent and adhere well to the substrate.

2.2 Characterization

The crystalline structure was analyzed by the PANalytical X'PERT Pro diffractometer using the Cu Kα radiation ($\lambda = 1.54059$A°) and a Ni filter at 40 kV and 20mA in the 2θ range (10–80°). The thicknesses measurements were carrying out in situ by a profilometer Altisurf®. This equipment uses a light source that contacts the sample; this process does not damage the sample. The morphology of thin films was observed by an atomic force microscope (A100-AFM) with non-contact mode. Elemental Analysis was performed using OXFord X-act Energy Dispersive X-ray Spectroscopy (EDX). The X-ray photoelectron spectroscopy (XPS) measurements were carried out with a SPECS DLD3500 Phoibos. The Raman spectra were recorded using a Santerra Bruker µ-Raman Spectrometer. The Optical properties were analyzed using a UV–visible spectrophotometer (Shimadzu, UV-3101) in the energy region of 2–6eV, while photoluminescence (PL) measurements were carried out by a Perkin-Elmer LS 50B luminescence spectrophotometer. The PL was measured at pumped helium temperature (1.2°K). The films was excited by an argon laser (ionized light Eexc = 3.47eV) with an output power of 20mW. The PL signals were detected with a photon counting system with a photomultiplier.

Table 1 The mean value of thickness for undoped and IZO thin films

	ZnO undoped	ZnO:0.5%In	ZnO:5%In	ZnO: 10%In
thickness	547nm	591 nm	591nm	418 nm

3 Results and Discussion

3.1 Structural properties

Figure 1 shows the XRD spectra of all the IZO thin films deposited on the glass substrate at various In doping concentrations.

It can be seen that all the films are polycrystalline with a hexagonal wurtzite-type structure. Undoped ZnO has (002) as the preferred orientation at $2\theta = 34.22°$. It is due to the minimal surface energy in the densest packed plane which, in the hexagonal structure, is the c-plane of the ZnO

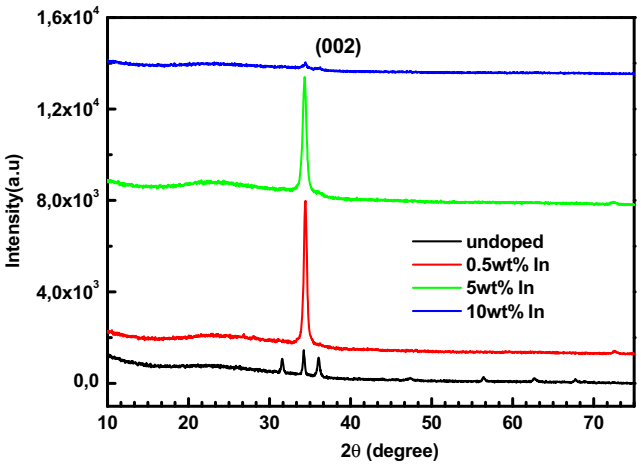

Fig. 1 The XRD patterns of the undoped and IZO thin films (0.5, 5 and 10%)

crystallites. This result is in good agreement with literature data [19, 20].

Other major peaks present are (100) and (101) at 2θ = 31.55° and 36.06° respectively, while other peaks like (102), (110), (103) and (112) at 47.39°, 56.42°, 62.70° and 67.75° respectively, are observed comparatively with lower intensities.

The IZO films with 0.5, 5 and 10wt% indium content, display sharp peaks, at 34.42° and 34.32° for 0.5, 5 and 10wt% respectively, maybe since ZnO crystals growing along the [002] direction, indicating the texture nature of the obtained films. This is due to the fact that the incorporation of Indium in the film favors the growth of the film according [002] direction. The crystallinity of the films deteriorated when indium content increased to 10wt% (the intensity of the (002) peak decreases drastically). Thus, preferential growth in the IZO films is strongly affected by the variation in the indium content.

Neither metallic zinc and indium characteristic peaks nor indium oxide peak were observed on any of the XRD spectra. Thus, the incorporation of indium does not alter the hexagonal structure of IZO films and does not initiate the formation of the In_2O_3 phase.

The grain size D is simply estimated by the Debye–Scherrer's formula:

$$D = \frac{0.9\lambda}{\beta cos\theta} \tag{1}$$

Where β is the full width at half maximum of the diffraction peak, 2θ is the Bragg angle and λ is the X-rays wavelength. The calculated values of D are listed in Table 2. The average grain sizes are found to be 37.20, 25.42, 22.15 and 13.44nm for 0, 0.5, 5 and 10wt% IZO thin films respectively.

The grain size decreased with increasing In content, indicating deteriorated the crystal quality of the film, which may be due to the formation of stresses by the difference in ion size between zinc (r_{Zn}^{2+} = 0.074nm) and the dopant (r_{In}^{3+} = 0.081nm) and the segregation of dopant in grain boundaries for high doping concentrations [21].

According to group theory, hexagonal wurtzite ZnO belongs to the C_{4V}^{6} space group. The optical phonons at the Γ point of the Brillouin zone are A1+2B1+E1+2E2.

Table 2 Variation of grain size for undoped and IZO thin films

	Grain size(nm)	Eg of ZnO (eV)	Eg of In_2O_3(eV)
undoped	37.20	3.21	-
0.5wt% In	25.42	3.15	3.73
5 wt% In	22.15	3.12	3.75
10 wt% In	13.44	3.14	3.78

Among these, the 2B1 modes are both infrared and Raman inactive (silent modes), they have two frequencies: B1(high) and B1(low) [22].

The A1 and E1 are polar modes and are both infrared and Raman active, they are split into transverse optical (TO) and longitudinal optical (LO) phonons, whereas the E2 modes are non polar and have two frequencies: E2(high) associated with oxygen displacement and E2(low) associated with the heavy Zn sub-lattice; both are Raman active. Each active vibration mode corresponds to a band in the Raman spectrum and the intensity of the band depends on the scattering cross section of the corresponding mode [22].

Figure 2 shows the typical Raman scattering spectra of undoped and IZO thin films observed at room temperature in the range from 120 to 1800 cm^{-1}. A peak located at 438cm^{-1} for 5 and 10wt% IZO thin films is observed in the spectrum. It can be assigned to the E2(high) mode of non-polar optical phonons; this is the intrinsic characteristic of the Raman-active mode of wurtzite hexagonal ZnO [28]. The E2(high) mode indicates the good crystallization of the IZO thin films in the hexagonal wurtzite structure, which further confirms the results of XRD analysis. On the other hand, the Raman spectrum of the 10wt% IZO thin films shows a weaker E2(high) peak in comparison to the 5wt% IZO thin films. The Raman spectrum of undoped ZnO and 0.5wt% IZO thin films exhibit no detectable E2(high) peak.

Usually, Raman peaks observed between 570 and 590cm^{-1} are considered to be associated with structural disorders, such as oxygen vacancies, Zn interstitials and their combination [22].

We observed on our Raman scattering spectra, the strong peak at 572cm^{-1}, corresponding to the E1(LO) mode, visible for undoped ZnO and 0.5wt% IZO thin films, is probably caused by the impurities and formation defects such as oxygen vacancies or oxygen-deficient regions [23].

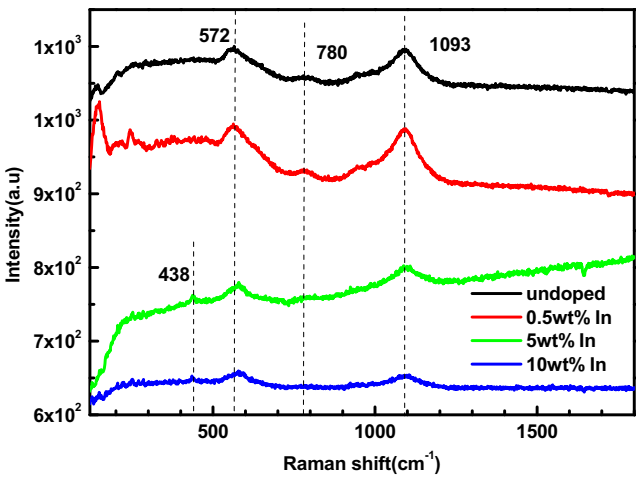

Fig. 2 Raman spectra of undoped and IZO thin films (0.5, 5 and 10%)

Therefore, the appearance of negligibly small E1(LO) peaks for the 5 and 10wt% IZO thin films indicates a fewer oxygen vacancies in these films.

In addition, two peaks located at 780 and 1093cm^{-1} may well correspond to multiple phonon scattering processes ($(E_2(high)–E_2(low))$ and A_{1T} mode, respectively) [24], and this strong multiple-phonon scattering is indicative of quantum confinement effect in our samples.

3.2 Morphological properties

It is also important to investigate the effect of In dopant concentration on the surface morphology of the films, which may affect the properties of the devices. AFM (atomic force microscopy) images of $3\times3\mu m^2$ scan areas on the films were taken in non-contact mode.

Two and three-dimensional AFM images of the surface morphology are given in Fig. 3 for 0, 0.5, 5 and 10wt% IZO thin films, respectively. It can be seen that the surface of 5wt% IZO thin films shows higher roughness and is less dense, and most of the irregularly rounded grains are separated from each other with voids. However, for 0.5 and 10wt% IZO thin films, the surface is relatively smooth and the spherical grains are uniformly and densely stacked up, which implies good crystallinity. The Indium incorporation in ZnO films significantly affects the surface morphology of the films. ZnO thin films with average thicknesses of 547 nm, 591 nm, 591 nm and 418 nm, of undoped and IZO thin films respectively, were obtained. The thickness decreases when the rate doping becomes 10%.(agreement with XRD results) Table 1.

EDS is performed to estimate quantitatively the doping concentration. The EDS data indicate that amounts of

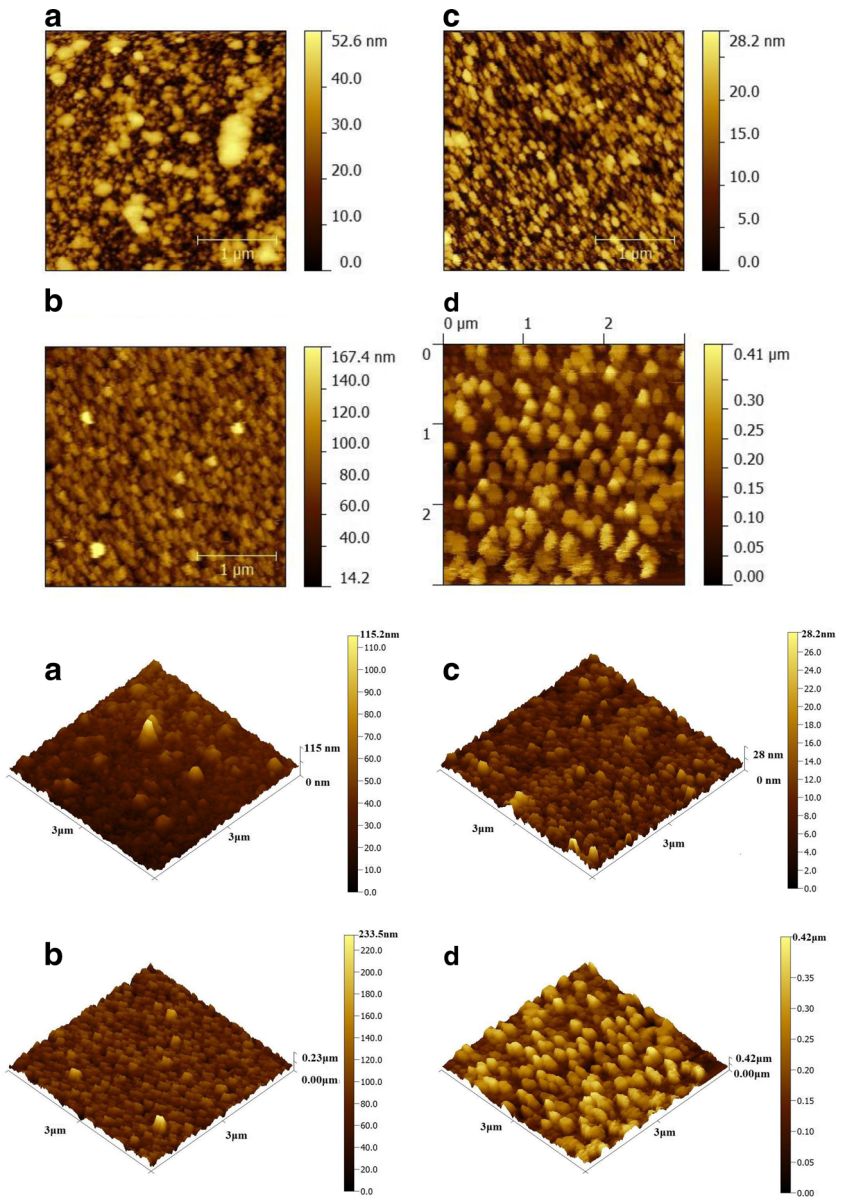

Fig. 3 AFM images of the samples **a** undoped; **b** 0.5; **c** 5 and **d** 10 wt% IZO thin films

Table 3 Quantitative analyzes of the EDS spectrum for undoped and IZO thin films

Element	undoped		0.5wt% In		5 wt% In		10 wt% In	
	wt%	Atomic%	wt%	Atomic%	wt%	Atomic%	wt%	Atomic%
Zn	43.93	19.10	18.23	6.65	38.90	16.45	15.31	5.54
O	31.15	55.35	39.13	58.34	32.01	55.30	39.77	58.76
In	-	-	-	-	1.19	0.29	2.13	0.44
Si	15.18	15.36	24.44	20.76	16.43	16.17	25.96	21.85
Na	5.58	6.91	7.96	8.26	6.76	8.13	7.98	8.20
Ca	3.45	2.45	5.27	3.14	3.57	2.46	5.35	3.15
Mg	0.71	0.83	1.42	1.39	0.90	1.02	1.39	1.35

indium introduced to the matrix of films are 0, 0, 0.29 and 0.44at% for 0, 0.5, 5 and 10wt% IZO thin films respectively (Table 3). Thus, the incorporation of Indium into the ZnO films is confirmed. The glass substrate, may be the originated of observed (Si, Na, Ca,..) elements.

In addition, the chemical bonding states of Indium ions in the IZO thin films were examined by X-ray photoelectron spectroscopy (XPS).The results are shown in Fig. 4, where Fig. 4a shows the full scanning region spectrum of the IZO samples (from 0 to 1200eV). Except for adventitious carbon (C_{1s}), only the characteristic peaks of Zn, O and In are observed in the spectrum, no other impurity phase was observed in the XPS analysis. The presence of the In peak confirm that indium ions have been incorporated in the ZnO lattice. In order to further verify the above mentioned statement, the high-resolution In_{3d}, Zn_{2p}, O_{1s} spectrum of IZO thin films are shown in Fig. 4b, c, d, respectively. From the scan, peaks detected at the energy positions of 440–460eV correspond to the In_{3d} orbital, their intensities confirm the EDS results. The high-resolution scan of In_{3d},

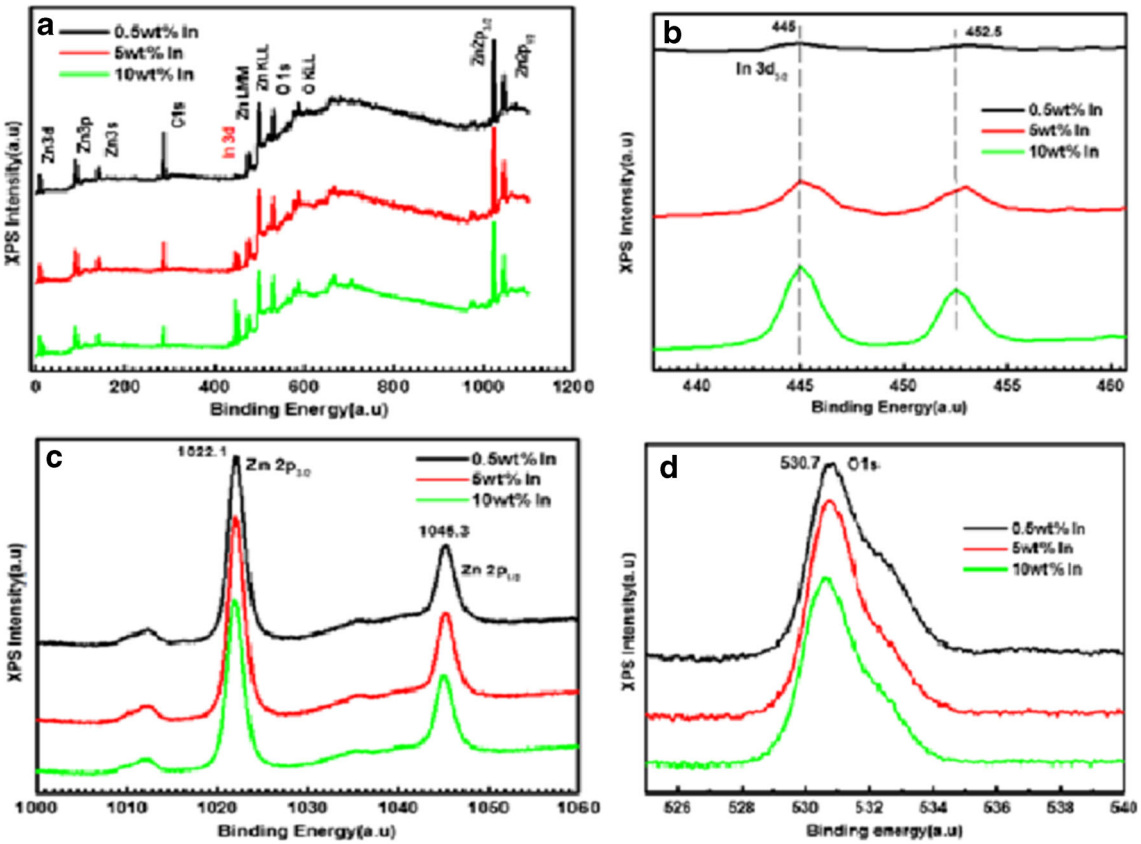

Fig. 4 XPS spectra of IZO thin films: **a** XPS spectrum of IZO thin films fully scanning from 0 to 1200 eV, **b** high resolution selective spectrum of In_{3d}, **c** high resolution selective spectrum of Zn_{2p}, **d** high resolution selective spectrum of O_{1s}

shown in Fig. 4b, identifies the exact peak location at 445eV, which is considered a feature of $In_{3d5/2}$ ions [25]. Given the proximity of the values corresponding to In_2O_3 and In_2S_3, and taking into account that the $In_{3d5/2}$ binding energy in In_2S_3 is included in the binding energy interval of $In_{3d5/2}$ in In_2O_3, it can't be established which of these two compounds is predominating [25]. The sharp and high symmetric peaks of $Zn_{2p3/2}$ and $Zn_{2p1/2}$ centered at 1022.1 and 1045.3eV, respectively are shown in Fig. 4c, with a spin orbital-splitting (D) of 23.2eV; this result confirms that Zn is present as Zn^{2+} [26]. The O_{1s} spectrum, Fig. 4d, exhibits an asymmetric feature indicating the presence of multi-component oxygen species on the surface of the sample [26]. The O_{1s} peaks corresponding to oxygen ions in a fully oxidized surrounding indicate that the relative quantity of the oxygen-vacancy related defects [27] is reduced with the incorporation of more Indium into the ZnO films.

Also, the O1s peak position shift to lower binding energies for 0.5, 5 and 10wt% IZO thin films is due to a decrease in the concentration of oxygen vacancies [28], which can influence the conductivity of oxide semiconductors and increase the background electron concentration [29]. Therefore, incorporating Indium reduces oxygen vacancies, indicating that In serves as the electron suppressor in ZnO films. Accordingly, we conclude that the In ions were successfully incorporated into the host ZnO lattice as In_{3d},which confirms the results obtained from EDS data and XRD analysis.

3.3 Optical properties

Figure 5 shows the transmittance spectra of the undoped and IZO thin films. We can see that optical transparency is higher than 70% in the visible region (400–700nm) of electromagnetic spectrum for all the IZO films, which gives them the character of transparency in the visible region and makes this material a potential candidate for optoelectronic applications. Despite, the absence of any characteristic peaks of indium oxide in XDR patterns, we can see two absorption edges, a strong clear one closed about 335 nm (3.7eV) and a weak salient absorption appear around 386 nm (3.2eV).

In the direct transition, the absorption coefficient can be expressed by [2]:

$$\alpha h\nu = A\sqrt{h\nu - Eg} \tag{2}$$

where A is a constant, α is a absorption coefficient, hν is a photon energy and Eg is a optical band gap. The plot of $(\alpha h\nu)^2$ vs hν is shown in Fig. 6. It can be seen that a extrapolation of the linear portion of the plot to the energy axis at $(\alpha h\nu)^2 = 0$ gives the optical band gap energy Eg. The obtained wide gaps (3.73, 3.75 and 3.78 eV for the 0.5, 5 and 10wt% indium doped ZnO thin films respectively) may be attributed to the absorption edge of the indium oxide (In_2O_3) . While, the lowest values of gaps (3.21, 3.15, 3.12 and 3.14 eV) can be attributed to the absorption edge of zinc oxide (ZnO).

Figure 7 shows the room-temperature photoluminescence emission spectra of the undoped ZnO film and the IZO thin films deposited at various In concentrations. The spectra exhibit various emission bands in different regions, and their asymmetric shape reveals the radiative emission happening in the specimens due to the presence of various ZnO native defects states. It can be seen that the undoped ZnO film shows the luminescence behavior of a narrow near band edge (NBE) emission centering at 380nm (3.26eV), which is weak in the case of the IZO thin films deposited at 0,5wt% Indium concentration. All the spectra exhibit strong defects-related visible emission peaks including violet emission at 408 nm (3.03eV) for undoped ZnO and at

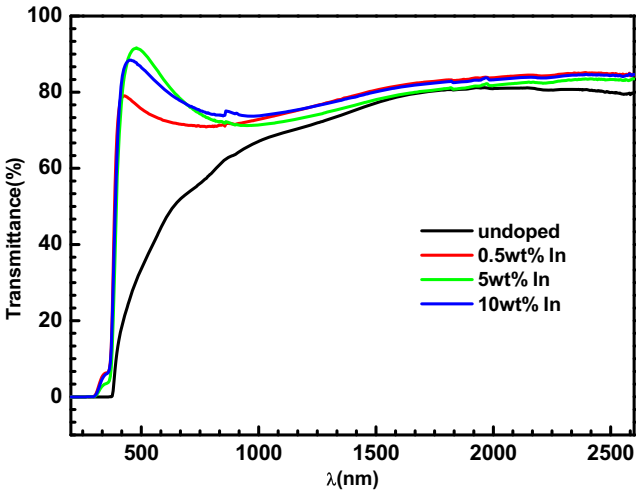

Fig. 5 Transmittance of undoped and IZO thin films (0.5, 5 and 10%)

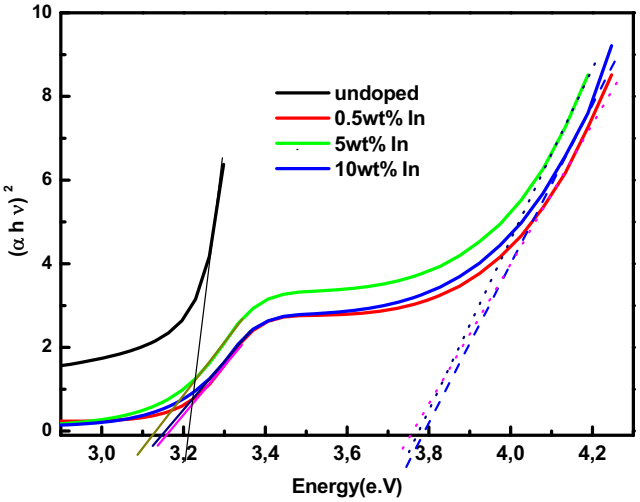

Fig. 6 Tauc's plots of undoped and IZO thin films (0.5, 5 and 10%)

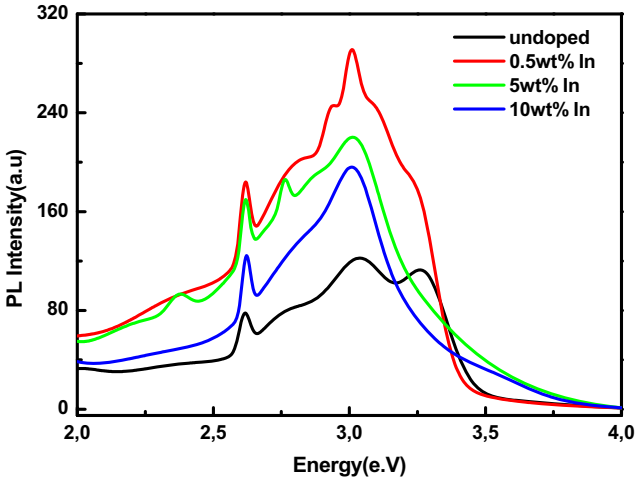

Fig. 7 Room temperature photoluminescence spectra of undoped and IZO thin films (0.5, 5 and 10%)

412nm (3.00eV) for the IZO films, blue emission at 448nm (2.76eV), blue–green emission at 473.5nm (2.61eV),and a deep level (DL) emission (green emission from 508nm (2.44eV) to 544nm (2.27eV)) for 5wt% IZO thin films. The intensity ratio of NBE-to-DL emission of the films is also dependent on the In concentration, and decreases with the increase in In doping concentration. This result reveals that more defects were generated in the IZO thin films. Similar behavior was observed by Kaul for Ga-doped ZnO prepared by MOCVD [30].

The NBE emission for the undoped ZnO and IZO thin films, originating from excitonic combination process, is related to the direct recombination of photo-generated carriers near the band edge. It is known that the NBE emission is commonly associated with the crystalline quality.

Accordingly, the crystalline quality of the deposited IZO thin films decreases with the increase of indium doping concentration due to the increased distortion of the crystal lattice by the extensive In concentration. Furthermore, the excess In atoms may reduce the NBE emission intensity by introducing either radiative deep levels or non-radiative channels.

The DL emission, which originates from the deep level of deficiency in the ZnO lattice, is probably related to the variation of the intrinsic defects in ZnO films. There are six kinds of intrinsic defects in ZnO films [31]: oxygen vacancy(VO), zinc vacancy(VZn), oxygen atom at the zinc position in the crystal lattice(OZn), zinc atom at the oxygen position in the crystal lattice(ZnO), interstitial oxygen(Oi) and interstitial zinc(Zni). All the films were deposited with 2-methoxyethanol, which suggests that the films should have a lot of oxygen vacancies (VO). As the radius of the zinc ion is much smaller than that of oxygen, the probability of interstitial oxygen (Oi) in ZnO lattice is very small.

4 Conclusion

Undoped and (0.5, 5, 10wt%) IZO thin films were prepared by sol gel method deposited on a glass substrate using the dip coating technique. The influence of doping concentration on structural, morphological, and optical properties was investigated. All films obtained have a wurtzite structure and preferred orientation along the [002] direction. Improvement in the films crystallinity are observed when the In rate doping with increasing up to 5 wt%. It was found that, as the indium concentration increases, the crystallite size decreases. The EDS and XPS results confirmed the incorporation of indium in the ZnO thin films. The transmittance spectra show that all films are highly transparent in the visible region. Room temperature PL measurements display NBE emissions, followed by defects-related emission peaks in the visible range attributed to defects and vacancies.

References

1. Benramache S, Benhaoua B (2012) Superlattices Microstruct 52:807–815
2. Khomchenko VS, Kryshtab TG, Savin AK, Zavyalova LV, Roshchina NN, Rodionov VE, Lytvyn OS, Kushnirenko VI, Khachatryan VB, Adame JAA (2007) Superlattices Microstruct 42:94–98
3. Venkatachalam S, Iida Y, Kanno Y (2008) Superlattices Microstruct 44:127–135
4. Rahmane S, Djouadi MA, Aida MS, Barreau N, Abdallah B (2010) Thin Solid Film 519:5–10
5. Park SM, Ikegami T, Ebihara K (2005) Jpn J Appl Phys 44:8027–8031
6. Ciobanu G, Carja G, Apostolescu G, Taraboanta I (2006) Superlattices Microstruct 39:328–333
7. Chia CH, Makino T, Tamura K, Segawa Y, Kawasaki M, Ohtomo A, Koinuma H (2003) Appl Phys Lett 82:1848–1850
8. Xu H, Liu Y, Mu R, Shao C, Lu Y, Shen D (2005) Appl Phys Lett 86:123–107
9. Yamada T, Nebiki T, Kishimoto S, Makino H, Awai K, Narusawa T, Yamamoto T (2007) Superlattices Microstruct 42:68–73
10. Duclère JR, Novotny M, Meaney A, O'Haire R, Mc Glynn E, Henry MO, Mosnier PJ (2005) Superlattices Microstruct 38:397–405
11. Benzaouk H, Drici A, Mekhnache M, Amara A, Guerione M, bernède JC, Bendjffal H (2012) Superlattices Microstruct 52:594–604
12. Ma J, Ji F, Ma HI, Li SY (1995) J Vac Sci Technol A13:92–94
13. Gu XQ, Zhu LP, Cao L, Ye ZZ, He HP, Chu PK (2011) Mater Sci Semicond Process 14:48–51
14. Teehan S, fstathiadis H, Haldar P (2011) J Alloys Compd 509:1094–1098
15. Kim D, Yun I, Kim H (2010) Curr Appl Phys 10:459–462
16. Park J, Lee C, Kim I, Jang S, Lee B (2009) Thin Solid Films 517:4432–4435
17. Sharma M, Mehra RM (2010) Thin Solid Films 518:3725–3730
18. Wang DY, Zhou J, Liu GZ (2009) J Alloys Compd 481:802–805

19. Luna-Arredondo EJ, Maldonado A, Asomoza R, Acosta DR, Melendez-Lira MA, de la L. Olvera M (2005) Thin Solid Films 490:132–136
20. Zi-qiang X, Hong D, Yan L, Hang C (2006) Mater Sci Semiconduct Process 9:132–135
21. Caglar Y, Ilican S, Caglar M, Yakuphanoglu F (2007) Spectrochim Acta A 67:1113–1119. https://doi.org/10.1088/0953-8984/23/33/334214
22. Calleja JM, Cardona M (1977) Phys. Rev. B 16:3753. https://doi.org/10.1103/PhysRevB.16.3753
23. Umar A, Kim SH, Lee H, Lee N, Hahn YB (2008) J. Phys D: Appl Phys 41:065412. https://doi.org/10.1088/0022-3727/41/6/065412
24. Fauteux C, Longtin R, Pegna J, Therriault D (2007) Inorg Chem 46:11036–11047
25. Wagner CD, Riggs WM, Davis LE, Moulder JF (1979) Handbook of X-ray Photoelectron Spectroscopy. Perkin Elmer, Eden Prairie, MN
26. Barick KC, Aslam M, Wu J, Dravid VP, Bahadur D (2009) J Mater Res 24:3543–3550
27. Seo SJ, Jeon JH, Hwang YH, Bae BS (2011) Appl Phys Lett 99:152102. https://doi.org/10.1063/1.3646388
28. Ku CJ, Duan ZQ, Reyes PI, Lu YC, Xu Y, Hsueh CL, Garfunkel E (2011) Appl Phys Lett 98:123511. https://doi.org/10.1063/1.3567533
29. King PDC, Veal TD, Phys J (2011) Condens Matter 23:334214
30. Kaul AR, Gorbenko OY, Botev AN, Burova LI (2005) Superlattice Microstruct. 38:272
31. Zhang SB, Wei SH, Zunger A (2001) Phys. Rev. B 63:075205. http://dx.doi.org/10.1103/PhysRevB.63.075205